# Flow Pressure Loss through Straight Annular Corrugated Pipes

**Joseph R. Sargent**[1]
Aerospace Systems And Propulsion (ASAP) Laboratory
Department of Mechanical and Aerospace Engineering
Florida Institute of Technology
150 W. University Blvd., Melbourne, FL 32901
sargent.joseph@gmail.com

**Daniel R. Kirk**[2]
Aerospace Systems And Propulsion (ASAP) Laboratory
Department of Mechanical and Aerospace Engineering
Florida Institute of Technology
150 W. University Blvd., Melbourne, FL 32901
dkirk@fit.edu

**Brandon Marsell**[3]
NASA Launch Services Center (LSP)
Kennedy Space Center, FL 32899
brandon.marsell@nasa.gov

**Jacob Roth**[4]
NASA Launch Services Center (LSP)
Kennedy Space Center, FL 32899
jacob.roth@nasa.gov

**Paul A. Schallhorn**[5]
NASA Launch Services Center (LSP)
Kennedy Space Center, FL 32899
paul.a.schallhorn@nasa.gov

**Brian Pitchford**[6]
Special Aerospace Services (SAS)
Kennedy Space Center, FL 32899

[1] Graduate Research Assistant
[2] Professor and Associate Dean for Research
[3] Environments and Launch Approval Branch
[4] Environments and Launch Approval Branch
[5] Chief, Environments and Launch Approval Branch
[6] Senior Systems Engineer

bpitchford@specialaerospaceservices.com

**Chris Webber**[7]
Special Aerospace Services (SAS)
Boulder, CO
cwebber@specialaerospaceservices.com

**Timothy Bulk**[8]
Special Aerospace Services (SAS)
Boulder, CO
tbulk@specialaerospaceservices.com

## ABSTRACT

Pressure loss through annular corrugated pipes, using fully developed gaseous nitrogen representing purge pipes in spacecraft fairings, was studied to gain insight into a friction factor coefficient for these pipes. Twelve pipes were tested: four Annuflex, four Masterflex and two Titeflex with ¼", 3/8", ½" and ¾" inner diameters. Experimental set-up was validated using smooth-pipe and showed good agreement to the Moody diagram. Nitrogen flow rates between 0-200 standard cubic feet per hour were used, producing approximate Reynolds numbers from 300-23,000. Corrugation depth varied from $0.248 \leq E/D \leq 0.349$ and relative corrugation pitch of $0.192 \leq P/D \leq 0.483$. Differential pressure per unit length was measured and calculated using 8-9 equidistant pressure taps. A detailed experimental uncertainty analysis, including correlated bias error terms, is presented. Results show larger differential pressure losses than smooth-pipes with similar inner diameters resulting in larger friction factor coefficients.

[7] Design Engineer & Analyst
[8] Chief Technical Officer and Co-Founder of Special Aerospace Services, LLC

## INTRODUCTION

Corrugated pipes are used in a wide array of supply flow and drain applications providing flexibility to accommodate bends and turns in the pipe while maintaining strength and rigidity. There are a variety of internal geometries of the corrugated pipes namely axial, annular (transverse), d-type and helical. Annular corrugated pipes can be sinusoidal, see Fig. 1, S-type [Fig. 2-left] or triangular [Fig. 2-right]. Fig. 1-left is a schematic representation of the internal geometry of a typical sinusoidal annular corrugated pipe and Fig. 1-right is a sample image of the corrugated pipes of three different diameters. The internal geometry of the corrugated pipes is characterized by the inner diameter, D, outer diameter, D+2E, corrugation height, E, and the corrugation pitch, P and the radius of each individual corrugation element, R.

One relevant application for corrugated pipes is to supply purging gases to a rocket launch vehicle payload fairing containing a spacecraft prior to launch. These specific braided stainless steel wrap reinforced pipes are able to withstand high internal pressures and temperatures. The purging gases, typically air or nitrogen, are used to keep instrumentation clean and to manage environmental conditions (temperature and humidity) inside the fairing. The diameters and lengths of the pipes vary based on mission specific flow purging requirements set by the size of the spacecraft in addition to various other parameters. For example, the supply pressure used to deliver the gas through the pipes must be adjusted to meet the flow rate and pressure limit constraints determined by the vehicle specifications. Adjusting flow requirements through valve sizing correlating to the given payload is challenging due to the inherent flow variations. This dictates that a flow analysis must be conducted prior to each mission in order to properly determine the correct valve settings for purging, and the a

key element of a trustworthy flow analysis is the knowledge of the friction factor, or pressure drop, for a given pipe geometry and flow rate.

Although corrugated pipes are used in many different engineering applications, the pressure drop and friction factor, as a function of pipe geometry and flow rate, are not readily available in the open literature. The standard Moody chart, which provides friction factor, f, versus the flow Reynolds number (based on hydraulic diameter) does not typically contain sand grain roughness values that are nearly as large as the ratio of corrugation element height to inner diameter, E/D. Further, limited experimental measurements indicate that the pressure drops are not in agreement with fully turbulent predictions and rough wall approximations even if the notion of the sand grain roughness analogy is extrapolated to E/D values consistent with typical corrugated pipes. Computational Fluid Dynamics (CFD) can be used to yield some estimates on the friction factor and pressure drop associated with the corrugated pipes, but these predictions would too benefit from experimental benchmarking.

The objective of the research presented in this work is to quantify the pressure loss per unit length and friction factor coefficient of a series of relevant corrugated pipes used in launch vehicle payload fairing environmental and purging applications for a series of corrugated pipes of several corrugation pitches, diameters, and flow rates representative of the functional range relevant to purging a spacecraft's payload fairing during mission operations. These data are then used to determine an appropriate friction factor to be implemented in simplified analytical and computational models of the purging system.

## THEORETICAL BACKGROUND AND LITERATURE REVIEW

A summary of the various sizes of corrugated pipe typically used in spacecraft fairing applications is provided in Table 1. Table 1 lists the important geometric parameters of the corrugated pipes, including inner diameter, D, outer diameter, D+2E, and the frequency of corrugation, which is defined as the number of corrugations per pipe length, S/L. and the radius of the corrugation, R. For spacecraft fairing applications, the flow rates of interest are 0-100 standard liters per minute (slpm) (or about 0 – 200 standard cubic feet per hour scfh) of nitrogen gas. For the diameters shown in Table 1 and for the maximum flow rate, the Reynolds number based on the inner diameter and based on the outer diameter is also summarized. For example, the smallest diameter pipe has a $Re_{ID}$ and $Re_{OD}$ of 21,590 and 13,530, respectively, at 200 scfh flow rate of nitrogen. The largest diameter pipe as a $Re_{ID}$ and $Re_{OD}$ of 6,765 and 4,416, respectively, at the 200 scfh flow rate of nitrogen.

Current launch vehicle payload compartment analysis requires the use of an estimated friction factor to approximate the pressure drop that occurs through the corrugated pipes. The friction factor is a measure of viscous loss for a flow in a pipe, and knowledge of the friction factor allows for estimation of the pressure drop per length associated with the pipe geometry and flow rate. For fully developed flow through a pipe, the Darcy-Weisbach equation (1) denotes the relationship for pressure drop over a length of pipe where f is the friction factor, L is the length of pipe, D is the hydraulic pipe diameter, $\rho$ is the density of the fluid, $V$ is the mean velocity of the flow.

$$\Delta P = f \frac{L}{D} \frac{\rho V^2}{2} \tag{1}$$

Friction factor dependence on Reynolds number and relative roughness was determined and named the Moody chart. For small Reynolds numbers (laminar flow, less than 2,300, friction factor can be determined by f=64/Re. The empirical relationship for turbulent flow in pipes (Re > 4,000) were calculated using the explicit Haaland approximation [3] to the Colebrook equation [11] given in (2)**Error! Reference source not found.**.

$$\frac{1}{\sqrt{f}} = -1.8\log\left[\left(\frac{\varepsilon/D}{3.7}\right)^{1.11} + \frac{6.9}{Re}\right] \tag{2}$$

Initially the corrugated pipes can be considered to have a relative (sand grain) roughness, ε/D, where ε=E and OD=ID+2E, which is also shown in Table 1. For example, the relative roughness associated with the smallest pipe is 0.30 and the relative roughness associated with the largest pipe is 0.26. These friction factors are outside of the relative roughness magnitudes that can be found, for example, on the Moody Chart for pipe friction with rough walls. However, even such an approximation can be useful to understand the differences is friction factor for a smooth pipe versus a flow with complete turbulence in a rough pipe.

In transverse corrugated pipes there are variances in geometric properties as shown in [Fig. 2]. There are few current papers concerning annular (transverse) corrugated pipes: Bernhard and Hsieh [9] investigated two plastic pipes and Popiel et al. [6] conducted experiments with four stainless steel corrugated pipes. Their studies are compared to our test matrix in Table 2. Both papers refer to S-type transverse corrugations and using water as the fluid while our study contained evenly spaced transverse corrugations as in Fig. *1* with gaseous nitrogen, but provide the closest approximation.

The vertical wall sections of pipe due to the corrugation of the piping make computational modeling inherently difficult because it relies on algorithms using average values of points in their surroundings. Jaiman [5] conducted CFD modeling for a sinusoidal transverse corrugation with a low corrugation pitch relative to inner diameter. Many other studies including [6] & [7] study d-type corrugations.

With an understanding of smooth internal wall and fully rough wall pipes, in laminar and turbulent flow Reynolds number regimes, an experimental set-up was specifically designed to determine the friction factors associated with the corrugated pipes shown in Table 1. The next section covers the experimental setup followed by the data parameters collected. After that details the smooth-line validation study of the experimental apparatus followed by the corrugated line results and an extensive section on uncertainty analysis of the experimental results is discussed. This study increases the accuracy of the flow prediction analysis to be utilized in future missions.

## EXPERIMENTAL SETUP

Fig. 3 shows a schematic of the experimental setup used to measure fluid differential static pressure at uniformly spaced fixed locations along a 3.05 meter (10 foot) length of corrugated pipe. The figure also shows important components, including the pressure regulator, relief valves, flow controllers, diffuser section, pressure transducers, data acquisition devices, and computer for data recording. To ensure that the flow was fully developed and free of entrance or exit effects, 0.61 meter (2 foot) extension segments attached with threaded fittings were attached to the entrance and exit of the primary test section pipe. Nitrogen flow

rate was controlled by two Alicat mass flow controllers (MC20 and MC 100, 20 and 100 standard liters/minute, respectively) with an accuracy of +/-0.8% of reading+0.2% of full scale.

To ensure that all pressure gauges and mass flow controllers were of sufficient sensitivity to accurately measure the pressure differential between the gauges a component selection study was performed. Two mass flow controllers were selected to minimize the error over the range of set points. Fig. 4 shows the percent error readings for the mass flow controllers. Fig. 5 shows the percent error readings for the differential pressure transducers with estimated differential pressure losses for the instrument only. The differential pressure readings were inadequate for the smallest diameter pipes due to a much larger readings than expected and a fifth differential pressure transducer was used to complete the data collection. A comprehensive uncertainty analysis was conducted and included in the last section of this paper.

A diffuser section between the flow controllers and test section ensured uniform flow from a smaller diameter supply source to a larger test section. The diffuser contained a brass muffler followed by a plenum chamber with a wire mesh screen at the end to ensure smooth, uniform flow through the pipes.

Typical static pressure ports for flow through pipes comprise of a smooth edge connection located on the outer surface or radially internal to the flow in a pitot static configuration. Given the unique configuration of the corrugated pipe geometry, static ports located on the outer diameter of the corrugated pipes could experience dynamic pressure as flow expands radially outward. Pitot static tubes required 15-20 times the diameter of the pitot tube to be engaged in the upstream flow. While properly designed static pitot tubes provide a

high degree of accuracy even when angular misalignment occurs [*10*], it was infeasible to install pitot static tubes with the small diameter pipes tested. A 22 gauge stainless steel needles 0.4064 mm ID, 0.7112 mm OD (0.016” ID, 0.028” OD) provided small interference to the flow and were adjusted to the center stream pipe for the static pressure measurement. A 6.35 mm (¼” NPT) hub provided connection to the pressure manifolds.

The distance between pressure port locations were approximately 304.8 mm (12 inches), but arranged to be drilled on the outer diameter and top outer peek of a corrugated segment. Custom 3D printed parts provided an accurate template for center punching, drilling holes and holding the needles into place. Needle position was maintained with holders holding the needle in the center of the drilled hole at the peak of the corrugation and the end of the needle was located in center stream of the pipe for various corrugations. After installation, the needles were sealed to the pipe using silicone and leak checked by pressure testing to 55.2 kPa (8 psi). The pressure taps attached to three-way switches then to two different manifolds – one designed as the high pressure side (upstream) and one low side (downstream). These high and low manifolds were connected in parallel to the Omega differential pressure transducers (summarized in Table 3) and simultaneously measured to ensure the proper range measurement. The burst pressure limit for the pressure transducers was 68.9 kPa (10 psi), which is 15% greater than the largest pressure loss recorded 58.6 kPa (8.5 psi).

## DATA RECORDING

Data was recorded for each pipe summarized in Table 1 by measuring the pressure differential between the following ports: 1-2, 1-3, 1-4, 1-5, 1-6, 1-7, 1-8, 1-9 and 1-10 for

nitrogen flow rates between 0-94.4 slpm (0-200 standard cubic feet per hour scfh) in increments of 4.72 slpm (10 scfh). An automated program was written in LabVIEW to cycle through the flow rates, for a single pair of port location inputs, and record all data. 30 seconds of data was the target time of steady state data taken for each configuration to ensure enough steady state data was taken. 40 seconds of each flow rate was selected to allow for sufficient settling time of the mass flow controller between flow rates. Data was collected continuously including this transient settling time. The user then switched selection of ports and re-ran the program, repeating this process for all differential pressure locations along the pipe. The mass flow controller data (volumetric flow rate (liters/min), mass flow rate (standard liters per minute), ambient temperature (°C) and ambient pressure (psia)) was collected at 10 Hz while the pressure transducers (in. $H_2O$) were sampled at 100 Hz.

To obtain independent sets of differential pressure readings for a set flow rate and port configuration the required the following data reduction steps:

1. Use the 'zero' flow measurement to re-zero all pressure transducer voltage readings
2. Truncate transient measurements between set point flow rates
3. Separate data according to flow rate

Since 4 pressure transducers were measured simultaneously, determine which pressure transducer was most accurate in range for a given flow rate

**SMOOTH-PIPE VALIDATION**

Electrical metal tubing (EMT) was used as a test flow pipe to validate the experimental apparatus by making pressure loss measurements and flow friction factor predictions. EMT

provided the rigidity, smoothness, and straightness for a test flow pipe, and a 15.875 mm ID and 20.955 mm ID (0.625" ID and 0.825" ID) tube were used. To ensure fully developed flow free from entrance or exit effects, a 5 foot long segment was attached to either end of the 10 foot test section. Fig. 6 and Fig. 7 show the measurement of differential pressure per unit length (kPa/mm) vs set point standard flow rates (standard liters per minute). Theoretical laminar and turbulent lines were recreated from the Haaland approximation (1) for smooth wall pipes and extended into the transitional region. The absolute roughness, $\varepsilon$, were adjusted in calculating the theoretical friction factor yielding 0.030 mm and 0.015 for Fig. 6 and Fig. 7 respectively. The error bounds calculations are detailed in the uncertainly analysis section below.

Fig. 8 shows the calculated friction factor vs Reynolds number for the smooth pipes. Friction factor was calculated using (3) where the average velocity was calculated using the standard volumetric flow rate divided by the cross sectional area. Reynolds number was calculated using (4).

$$f = \frac{\Delta P}{L}\frac{2D}{\rho V^2} \tag{3}$$

$$Re = \frac{DV\rho}{\mu} \tag{4}$$

Both pipes show a high degree of agreement between theoretical calculations and experimentally measured data for both differential pressure vs flow rate and transformation to friction factor vs Reynolds number – proving the experimental setup valid.

**CORRUGATED PIPES DATA**

For each of the varying flow rate set points, differential pressure port locations, and pipe conditions described in the data recording section, differential pressure and flow rate were collected. Fig. 9 shows a sample of steady state flow rate (slpm) and differential pressure (kPa) data sampled over 30 seconds for a single port configuration. Fig. 9-top shows the randomness of the differential pressure readings over time. Fig. 9-left shows the mass flow controller readout vs time and Fig. 9-right shows the differential pressure vs flow rate. The uniformity of the measured parameters is apparent in all three sections of the figure and throughout the experimentation data.

The data was then condensed time-wise and normalized by length into Fig. 10 which displays the differential pressure per unit length kPa/mm for each of the 9 port locations. The spread of measurements was more apparent when differential pressure measurements were lower in the range of the pressure transducer selected. Overall, the spread of normalized differential pressure readings per unit length were minimal to the overall scale of pressure readings (note the relatively small scale on the y-axis). Observations of independent needle installation error became apparent from these plots (discussed later in the uncertainty analysis) and excluded in report. Discussion on needle position and differential pressure reading error is elaborated in the uncertainty analysis section.

Through the use of equations (3) & (4), friction factor and Reynolds number can be calculated for each of the test conditions of the corrugated pipes. Finally, Fig. 11 shows an approximation of the friction factor vs Reynolds number for all of the corrugated pipes. Friction factor for the laminar region was included in the plot as a reference. The corrugated pipes show

good agreement for approximate Reynolds numbers typically found in the laminar flow regime for smooth-wall pipes (Re < 2,300). The authors believe that the variation is due to the slight angular misalignment of the first needle which was used as a reference for the entire experiment. For larger Reynolds numbers near the smooth-wall pipe turbulent region (Re > 4,000), the corrugated pipes tested show a decrease of friction factor with increasing Reynolds numbers. There are also several pipes which show the same relationship as Popiel, et. al [6] and Bernhard and Hsieh [9] where the friction factor increases with increasing Reynolds number.

## UNCERTAINTY ANALYSIS

Using methodology described by Coleman and Steele [1], uncertainty was determined for the measured average of the differential pressure per unit length. Equation (5) quantifies the general uncertainty of any result, r, where $B_x$ are the individual systematic errors and $P_x$ are the random error effects. Governing equation (6) determines the average differential pressure per unit length of a given pipe where n is the number different port lengths tested, $\Delta P_{1\text{-}j}$ is the differential pressure measurement and $\Delta d_{1\text{-}j}$ is the length measurement from port 1 to port j.

$$\left(\frac{U_r}{r}\right)^2 = \sum_{i=1}^{J}\left\{\left(\frac{\partial r}{\partial X_i}\right)^2 B_i^2\right\} + 2\sum_{i=1}^{J-1}\sum_{k=i+1}^{J}\left\{\left(\frac{\partial r}{\partial X_i}\right)\left(\frac{\partial r}{\partial X_k}\right)[B_i B_k]_{correlated}\right\} + \sum_{i=1}^{J}\left\{\left(\frac{\partial r}{\partial X_i}\right)^2 P_i^2\right\} + 2\sum_{i=1}^{J-1}\sum_{k=i+1}^{J}\left\{\left(\frac{\partial r}{\partial X_i}\right)\left(\frac{\partial r}{\partial X_k}\right)[P_i P_k]_{correlated}\right\} \tag{5}$$

$$r \stackrel{\text{def}}{=} \left(\frac{\Delta P}{L}\right)_{Avg} = \frac{1}{(n-1)}\sum_{j=2}^{n}\left(\frac{\Delta P_{1-j}}{d_{1-j}}\right) \tag{6}$$

### Elemental Bias Sources

From ISO guide to the expression of Uncertainty and Measurements [4], $u_X$ is found from the combination of all the standard elemental uncertainties as described in equation (7):

$$(u_X)^2 = (u_1)^2 + (u_2)^2 + (u_3)^2 + (u_4)^2 + (u_5)^2 \tag{7}$$

The following were identified as possible elemental bias sources in the uncertainty of the result:

1. Pressure Transducers (summarized in Table 3) where the relative biased of the pressure transducer to the maximum reading (worst-case full scale assumed) is given by equation (8).

$$\left(\frac{b_{PT}}{PT}\right)_{MAX} = \frac{Linearity * Range}{MAX\ Reading} \tag{8}$$

2. Distance between pressure probes with a tape measure with a precision 1.5875 mm (1/16”) with a range of 7.315 meters (24 ft.) Adapting equation (8) for the distance measurement would yield $b_{\text{tape measure}}$ = 0.0625” and a relative bias of 0.0052 = 0.0625”/12”.

*Differential Pressure Bias*

The overall biased ($b_{\Delta P_{1-n}}$) associated with measuring difference in pressure between holes 1 and n using equation (7) with elemental sources $b_{Pressure\ Transducer}$ is the biased from the pressure transducer itself, $b_{DAQ}$ is the biased associated with the data acquisition and $b_{P-Installation}$ is the biased with installation effects. The biased associated with the Data Acquisition System (16 bit resolution, -10V to 10V analog inputs) yields $b_{DAQ}$ = 20V / 2^16 = 0.000305 V, with a relative bias of 0.000305V/5.00V = 0.0000610.

Pressure transducer installation ($b_{P-Installation}$) effects were estimated by the following considerations: 1) angle of needles with respect to nominal flow direction. Assuming 2 degrees misalignment for both needles at location 1 and n and swaying of needles due to flow (resonance/helm holds/vortices) (1%). Combination of elemental sources by (7), ($b_{P-Installation}$) yielding a maximum worst case relative bias for the differential pressure readings of 0.0141 or 1.41%.

*Distance Between Ports Bias*

Biased associated with measuring distance between holes ($b_{d_{1-n}}$) include elemental sources of the bias of the tape measure and biased associated with installation effects:

The following distance installation errors effects were considered and estimating the following considerations: 1) linear offset of needles – assumed negligible due to installation and holder design, 2) angle of needle would produce a small linear offset: Assuming a total of 10 degrees off with a needle length of 15.24 mm (0.6”) would yield: $b_{angle}$ = 15.24*tan(10) = 2.67 mm (0.105”), 3) Straightness. Assuming two arc-lengths with a maximum deviation of 6.35 mm (0.25”) over a 317.5 mm (12.5”Z) span, would yield $b_{straightness}$ = (arc-length – original length) = 318.85 mm – 317.5 mm (12.553”-12.5”) = 1.35 mm (0.053”), 4) Concentricity of needle and corresponding hole: the hole size was drilled to 1.19mm (3/64”, 0.046875”) while the needle OD is 0.711 mm (0.028”). The range would then be: 1.19 mm-0.711 mm = 0.0479 mm (0.046875”- 0.028” = 0.019”) or 0.00mm +/- 0.241 mm (0.000” +/- 0.0095”). The smallest distance being 304.8 mm (12.000”) in between holes would give a biased of: $b_{concentric}$ = 0.241 mm*2 holes = 0.482 mm (0.0095”*2 holes = 0.019”). The biased associated with installation

effects would yield $b_{L\text{-installation}}$ = 3.03 mm (0.1191”) and the biased associated with the distance between pressure ports is $b_{d_{1-n}}$ = 3.42 mm (0.1345”).

**Combined Biased Sources**

Assume that the following pairs of bias terms are perfectly correlated:

$\Delta P_{1-j}$ $and$ $\Delta P_{1-k}$ when the same pressure transducer is used for j and k measurements

All $d_{1-j}'s$ with all other $d_{1-k}'s$ ,

All other terms are not correlated ($\Delta P_{1-j}$ $wrt.$ $d_{1-k}'s$).

Using [1, Eq. 5.17, p. 145], the number of elemental error sources that are common is one for both delta pressure measurement and distance measured the correlated bias error for differential pressure is given by equation (9) which yields $b^2_{\Delta P_{1-j}\Delta P_{1-k}}$ = 128,400 Pa$^2$ (0.0027 psi$^2$) and for distance by equation (10) $b^2_{d_{1-j}d_{1-k}}$ = 1.632 mm$^2$ (0.00253 in$^2$).

$$b^2_{\Delta P_{1-j}\Delta P_{1-k}} = \left(b_{\Delta P_{1-j}}\right)\left(b_{\Delta P_{1-k}}\right) \tag{9}$$

$$b^2_{d_{1-j}d_{1-k}} = \left(b_{d_{1-j}}\right)\left(b_{d_{1-k}}\right) \tag{10}$$

**Revised Biased Equation**

Assuming no precision length uncertainty and no correlate precision error with precision pressure transducer ($P^2_{\Delta P_{1-j}}$) determined to 95% confidence interval using 2*standard deviation of measurements collected, the following overall uncertainty can be calculated as equation (11):

$$\left(\frac{U_{\left(\frac{\Delta P}{L}\right)_{Avg}}}{\left(\frac{\Delta P}{L}\right)_{Avg}}\right)^2 = \left(\frac{1}{(n-1)}\right)^2 \sum_{j=2}^{n}\left[\left(\frac{b^2_{\Delta P_{1-j}}}{d^2_{1-j}}\right)\right] + \left(\frac{1}{(n-1)}\right)^2 \sum_{j=2}^{n}\left[\left(\frac{\Delta P_{1-j}}{(d_{1-j})^2}\right)^2 b^2_{d_{1-j}}\right]$$
$$+\ 2\left(\frac{1}{(n-1)}\right)^2 \sum_{j=2}^{n}\sum_{k\neq j}\left[\left(\frac{1}{d_{1-j}}\right)\left(\frac{1}{d_{1-k}}\right) b^2_{\Delta P_{1-j}\Delta P_{1-k}}\right]$$
$$+\ 2\left(\frac{1}{(n-1)}\right)^2 \sum_{j=2}^{n}\sum_{k\neq j}\left[\left(\frac{\Delta P_{1-j}}{(d_{1-j})^2}\right)\left(\frac{\Delta P_{1-k}}{(d_{1-k})^2}\right) b^2_{d_{1-j}d_{1-k}}\right]$$
$$+\left(\frac{1}{(n-1)}\right)^2 \sum_{j=2}^{n}\left[\left(\frac{P^2_{\Delta P_{1-j}}}{d^2_{1-j}}\right)\right] \tag{11}$$

Nominal relative error for all test scenarios were around 20% with a few notable exceptions. The lower the flow rate, the more relative error in the measurements. The smaller the diameter, the greater the flow rate which also increased the relative error as much as 70-80%.

## CONCLUSIONS

This study developed a method of measuring differential pressure per unit length of corrugated pipes of various diameters, geometries, and manufacturers. The method was tested on 12 different pipes of which ten were corrugated and two were smooth to develop a measurement for differential pressure per unit length. The apparatus was validated within ~10% of theoretical flow loss calculations.

From the results gained, the data is showing that the flow loss difference between smooth and corrugated pipes are greater than expected. The following conclusions were reached:

1. Test apparatus was created to measure differential pressure of pressure tap locations on different pipes.
2. The apparatus was validated within ~10% of theoretical flow loss calculations.

3. Differential pressure loss was measured for various corrugated pipes.
4. A sufficient amount of data points were collected to produce an accurate calculation and uncertainty analysis was conducted on the results.

All studies performed used straight pipe testing. The authors understand secondary flow effects through bending the pipes with various bend angles and radii. The authors also plan to use the data set to develop a friction factor relationship for corrugated geometry. This study obtained empirical data via pressure measurements of corrugated pipes of various diameters, geometries, and flow rates and conduct a comparison analysis of smooth pipes of similar diameters.

**ACKNOWLEDGMENT**

NASA LSP

**FUNDING**

NASA Launch Services Program (NASA LSP) awarded contract NNK14522002R to Special Aerospace Services, LLC of Boulder, CO who subcontracted Florida Institute of Technology to conduct this study.

**NOMENCLATURE**

| | |
|---|---|
| $b_x$ | Estimate of the standard deviation of the distribution of the parent population from which a particular systematic error originates. |
| $D$ | Inner diameter of corrugated pipe |
| $d_{1-j}$ | Distance between port 1 and port j |
| E | Corrugation height |
| $f$ | Friction factor |
| n | Total number of pressure ports installed on a pipe |
| n | Total number of pressure ports installed on a pipe |
| $\Delta P_{1-j}$ | Differential pressure measurement between port 1 and port j |
| $P^2_{\Delta P_{1-j}}$ | 2*standard deviation of differential pressure readings |
| r | Result defined as the average differential pressure per unit length |
| R | Corrugation element radius |
| Re | Reynolds number |

**REFERENCES**

[1] Coleman, Hugh W., and W. Glenn Steele. Experimentation, Validation, and Uncertainty Analysis for Engineers. 3rd ed. Hoboken, N.J.: John Wiley & Sons, 2009. ISBN: 978-0-470-16888-2

[2] Munson, Bruce Roy, and T. H. Okiishi. Fundamentals of Fluid Mechanics. 6th ed. Hoboken, NJ: J. Wiley & Sons, 2009. ISBN: 978-0-470-16888-2

[3] Haaland, S. E., 1983, “Simple and Explicit Formulas for the Friction Factor in Turbulent Pipe Flow,” ASME J. Fluids Eng., 105, pp. 89–90. DOI: 10.1115/1.3240948

[4] International Organization for Standardization (ISO), Guide to the Expression of Uncertainty in Measurement, ISO, Geneva, 1993. Corrected and reprinted, 1995.

[5] Jaiman, Rajeev K., Owen H. Oakley, Jr., and J. Dean Adkins. 2010. "CFD Modeling of Corrugated Flexible Pipe." Proceedings of the OMAE2010 29th International. Shanghai, China. DOI:10.1115/OMAE2010-20509

[6] Popiel, C. O., M. Kozak, J. Malecka, and A. Michalak. 2013. "Friction Factor for Transient Flow in Transverse Corrugated Pipes." Journal of Fluids Engineering. DOI: 10.1115/1.4023945

[7] Stel, Henrique, Rigoberto E. M. Morales, Admilson T. Franco, Silvio L. M. Junqueira, Raul H. Erthal, and Marçelo A. L. Goncalves. 2010. "Numerical and Experimental Analysis of Turbulsnet Flow in Corrugated Pipes." Journal of Fluids Engineering. DOI: 10.1115/1.4002035

[8] Vijiapurapu, Sowjanya, and Jie Cui. 2007. "Simulation of Turbulent Flow in a Ribbed Pipe Using Large Eddy Simulation." Numerical Heat Transfer, Part A: Applications: An International Journal of Computation and Methodology.

[9] Bernhard, D. M. and Hsieh, C. K. “Pressure Drop in Corrugated Pipes.” 1995. Journal of Fluids Engineering. DOI: 10.1115/1.2817393

[10] Mitchell, W., B. Blagun, D. Johnson, and M. Midgett. “Angular Flow Insensitive Pitot Tube Suitable for use with Standard Stack Testing Equipment.” U.S. Environmental Protection Agency, Washington, D.C., EPA/600/4-79/042 (NTIS PB80102007).

[11] Colebrook, C. F., 1939, “Turbulent Flow in Pipes With Particular Reference to the Transition Region Between the Smooth and Rough Pipe Laws,” J. Inst. Civ. Eng. London, 11, pp. 133–156.

**Figure Captions List**

Fig. 1 Corrugated pipe geometry and photo of sample corrugated pipes

Fig. *2* Variations in transverse corrugated pipes

Fig. 3 Schematic diagram of experimental setup

Fig. 4 Measurement error for mass flow controller

Fig. 5 Measurement error differential pressure transducers

Fig. 6 0.625" ID EMT pressure loss per unit length (kPa/mm) vs flow rate (standard liters/minute)

Fig. 7 0.825" ID EMT pressure loss per unit length (kPa/mm) vs flow rate (standard liters/minute)

Fig. 8 Smooth pipe friction factor vs Reynolds number

Fig. 9 Sample data pipe #17 at 70 scfh plot of: flow rate vs time (upper left), differential pressure vs time (upper right), and differential pressure vs flow rate (bottom) (step 4)

Fig. 10 Sample Data Pipe #17 @ 70 scfh plot of differential pressure per unit length for ports (different lengths) tested (step 5)

Fig. 11 Estimation of friction factor vs Reynolds number for corrugated pipes

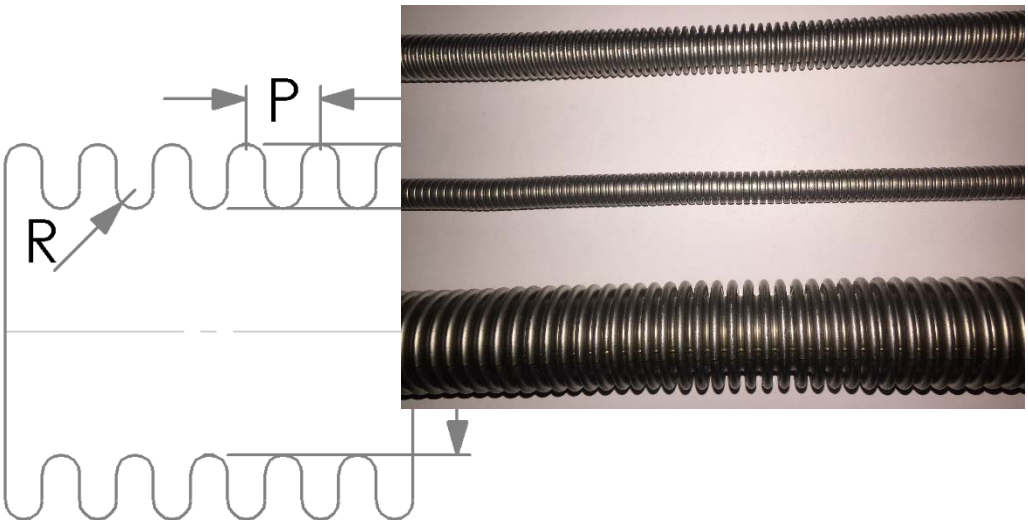


Fig. 1

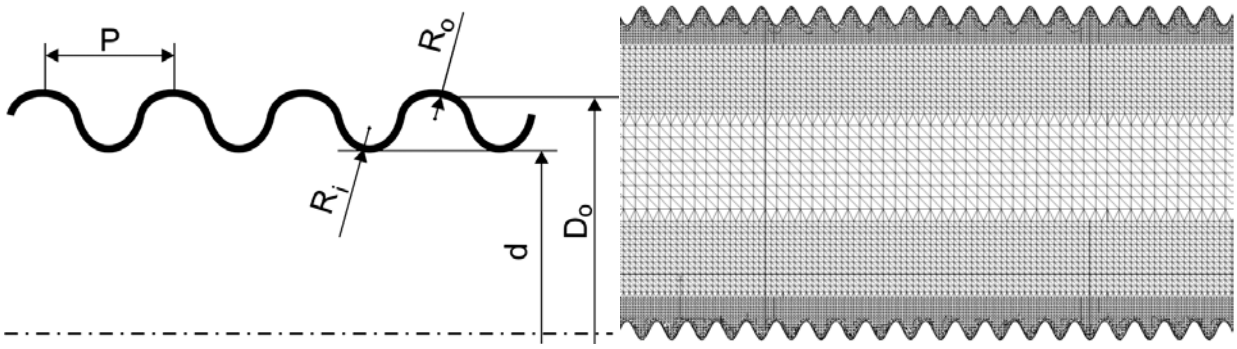


Fig. 2

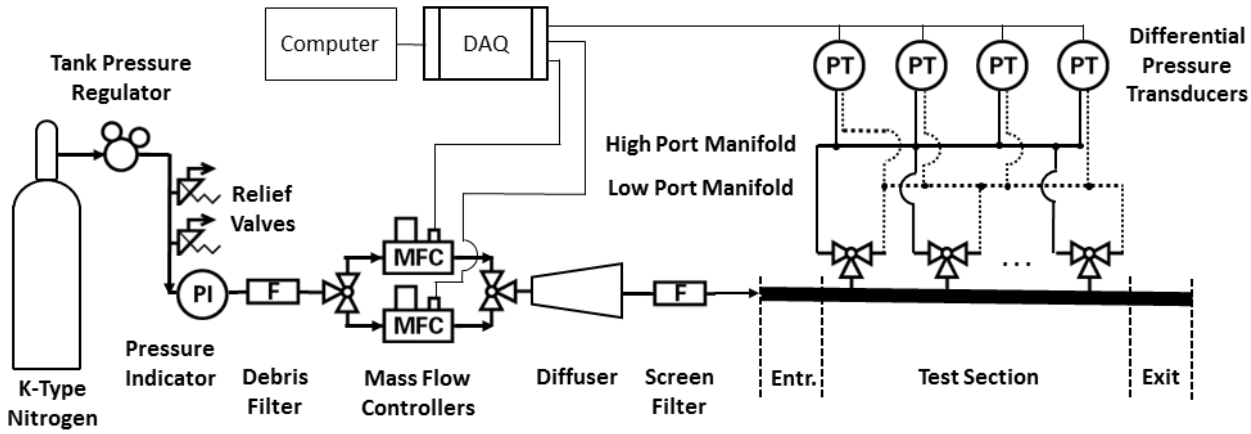
Computer
DAQ
Tank Pressure Regulator
Differential Pressure Transducers
PT
PT
PT
PT
High Port Manifold
Low Port Manifold
Relief Valves
MFC
MFC
PI
F
F
K-Type Nitrogen
Pressure Indicator
Debris Filter
Mass Flow Controllers
Diffuser
Screen Filter
Entr.
Test Section
Exit

Fig. 3

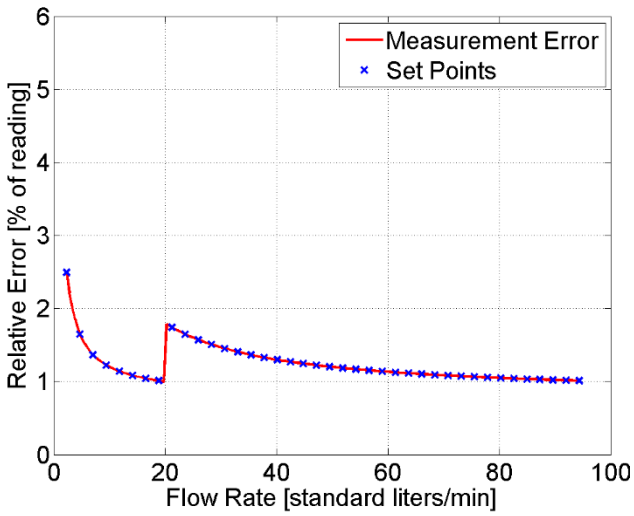
Measurement Error
Set Points
Relative Error [% of reading]
Flow Rate [standard liters/min]
0
1
2
3
4
5
6
0
20
40
60
80
100

*Fig. 4*

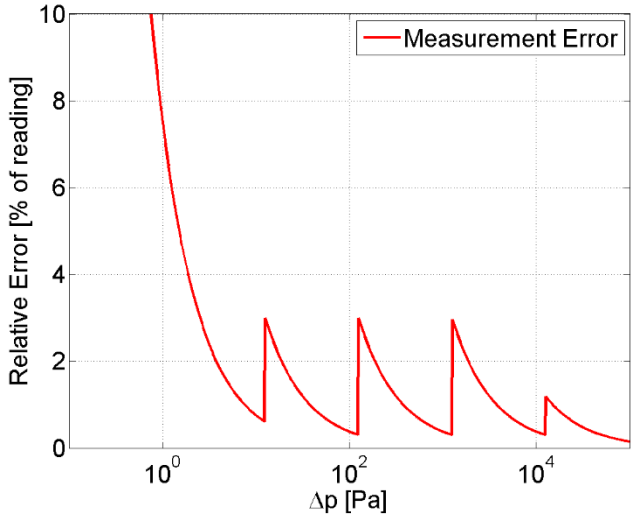
Measurement Error
Relative Error [% of reading]
10
8
6
4
2
0
$10^0$
$10^2$
$10^4$
Δp [Pa]

*Fig. 5*

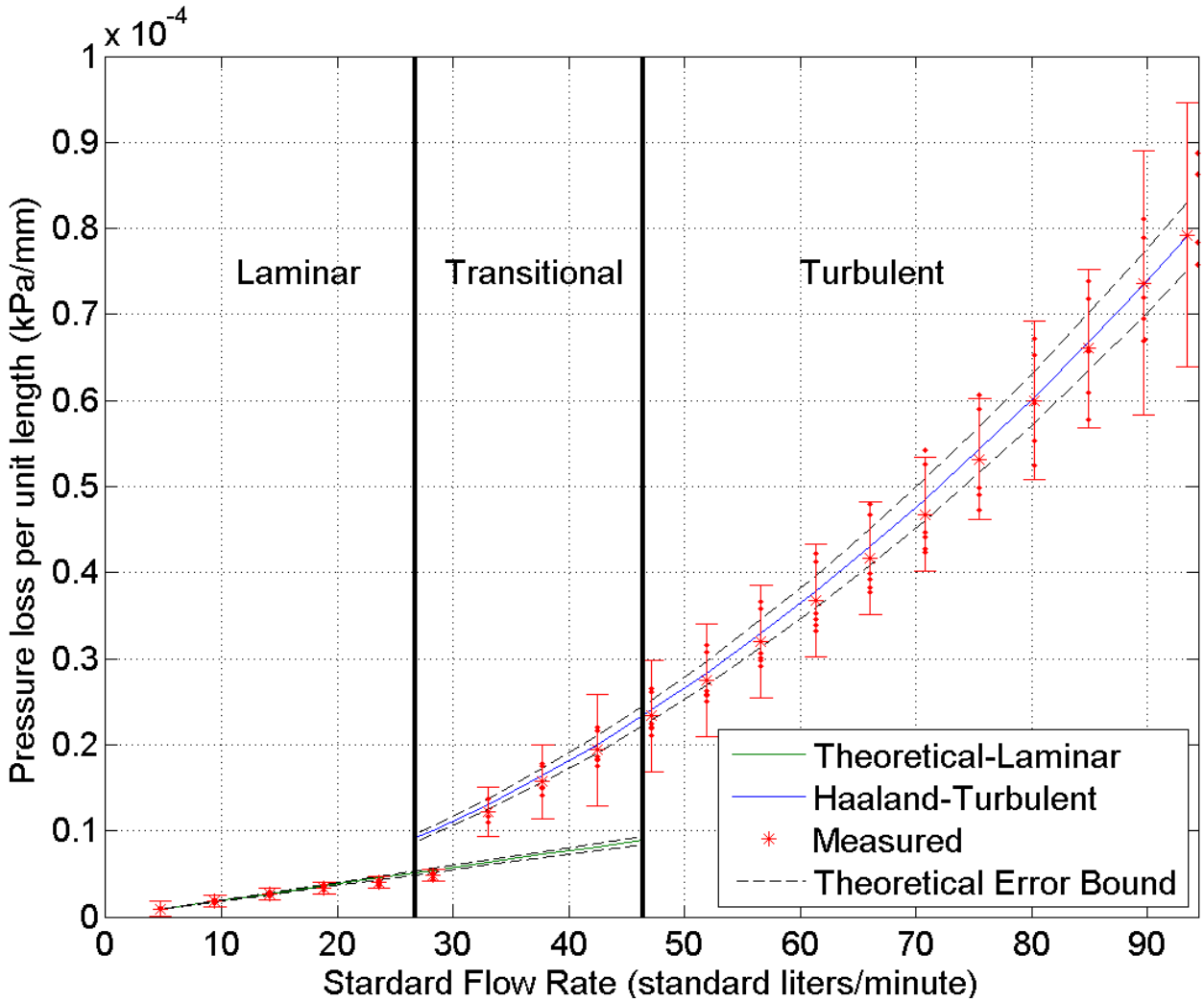
x 10^-4
Pressure loss per unit length (kPa/mm)
Stardard Flow Rate (standard liters/minute)
Laminar
Transitional
Turbulent
Theoretical-Laminar
Haaland-Turbulent
Measured
Theoretical Error Bound
0
0.1
0.2
0.3
0.4
0.5
0.6
0.7
0.8
0.9
1
0
10
20
30
40
50
60
70
80
90

Fig. 6

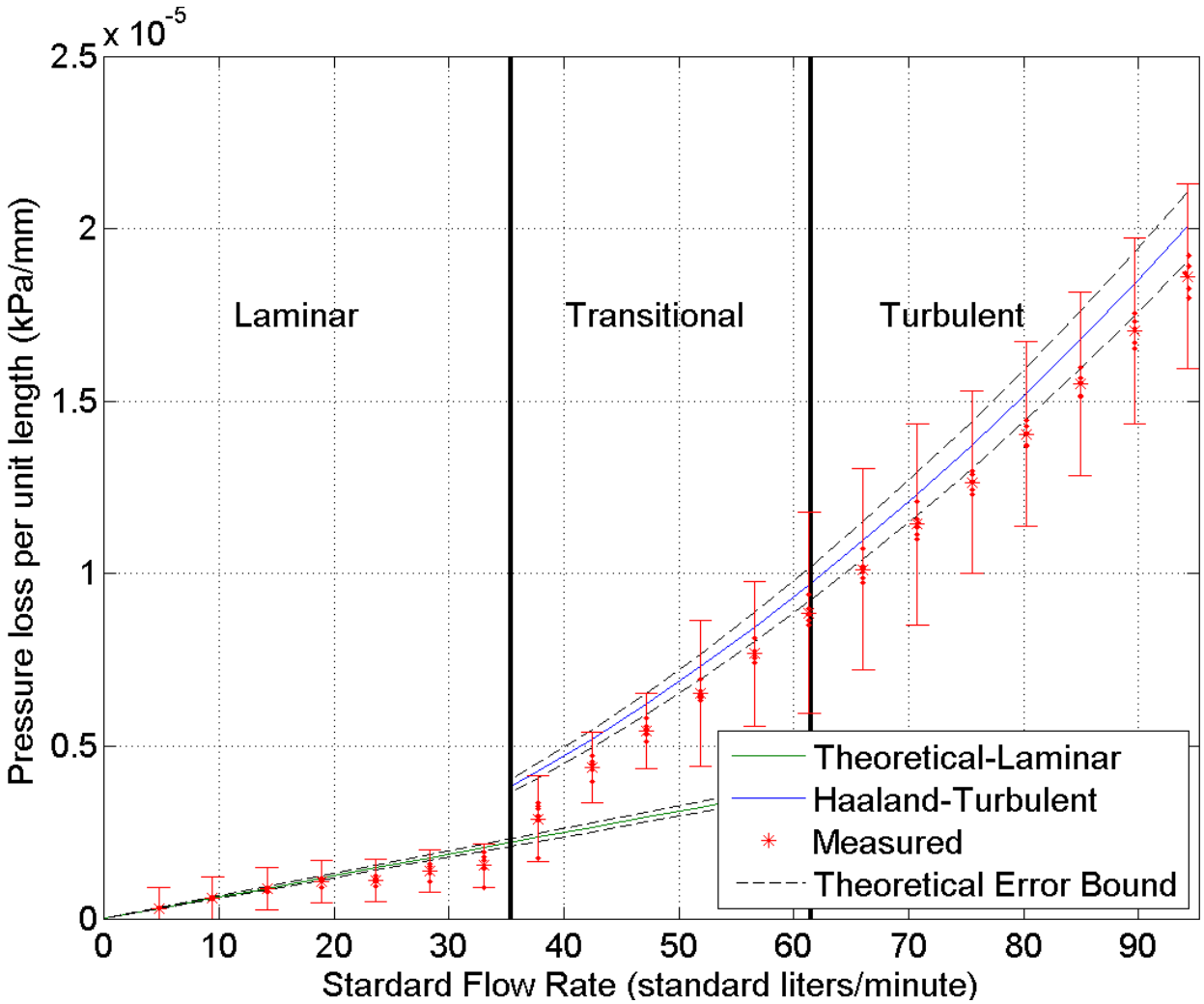
x 10^-5
2.5
2
1.5
1
0.5
0
Pressure loss per unit length (kPa/mm)
Laminar
Transitional
Turbulent
Theoretical-Laminar
Haaland-Turbulent
Measured
Theoretical Error Bound
0
10
20
30
40
50
60
70
80
90
Stardard Flow Rate (standard liters/minute)

Fig. 7

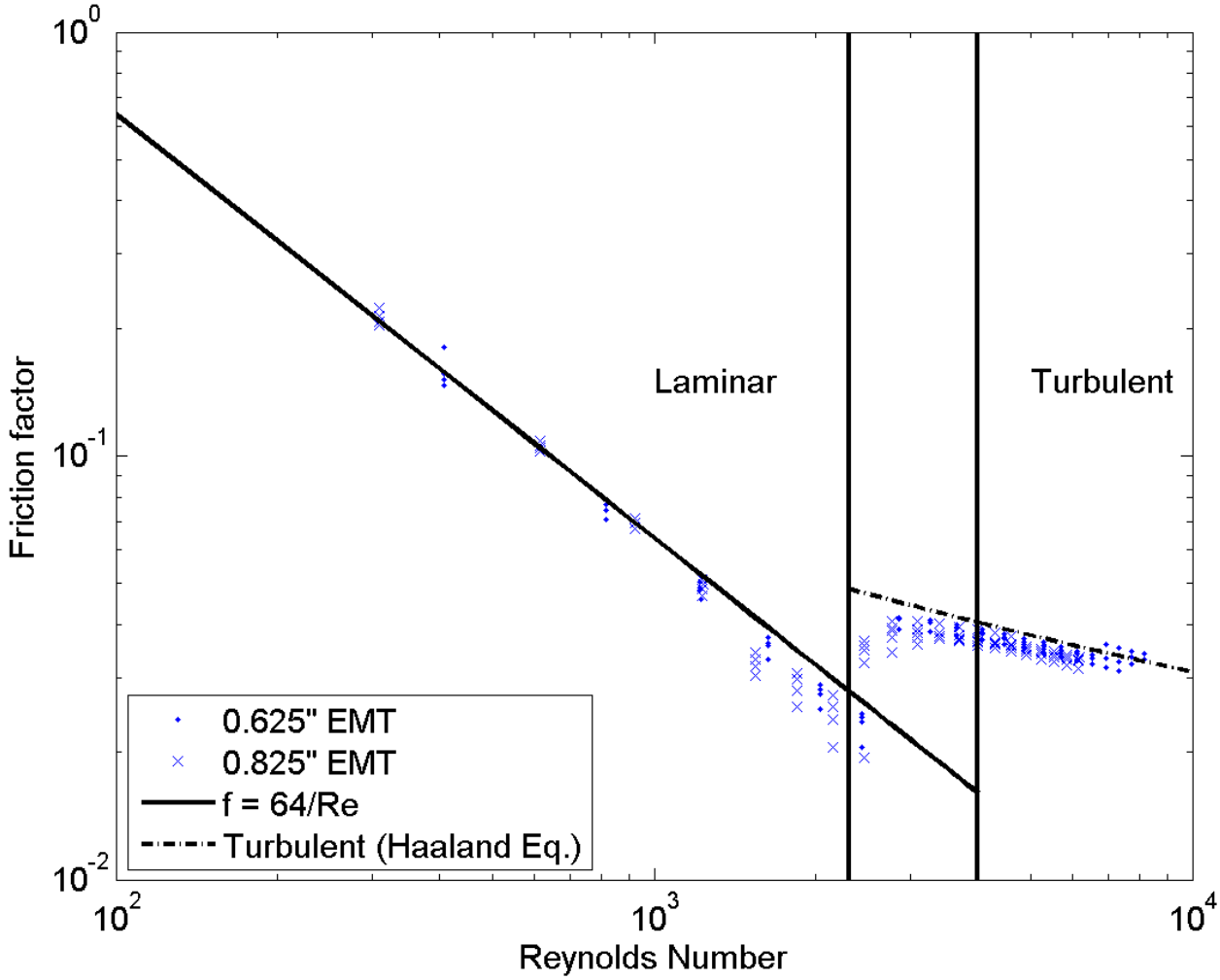
Friction factor
Reynolds Number
Laminar
Turbulent
0.625" EMT
0.825" EMT
f = 64/Re
Turbulent (Haaland Eq.)

*Fig. 8*

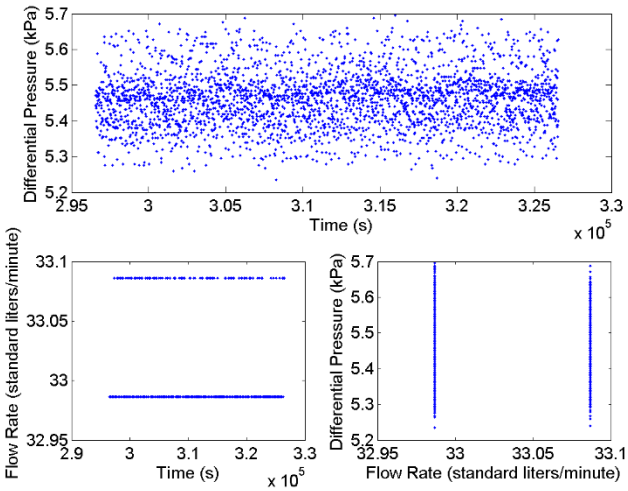
Differential Pressure (kPa)
5.7
5.6
5.5
5.4
5.3
5.2
2.95
3
3.05
3.1
3.15
3.2
3.25
3.3
Time (s)
x 10^5
Flow Rate (standard liters/minute)
33.1
33.05
33
32.95
2.9
3
3.1
3.2
3.3
Time (s)
x 10^5
Differential Pressure (kPa)
5.7
5.6
5.5
5.4
5.3
5.2
32.95
33
33.05
33.1
Flow Rate (standard liters/minute)

*Fig. 9*

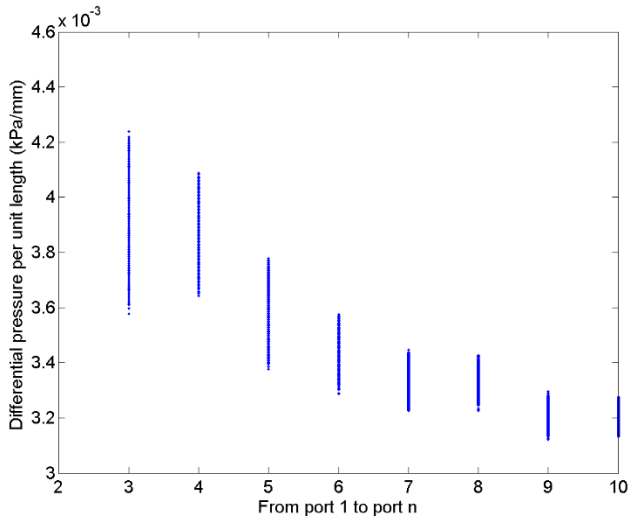
x 10^-3
4.6
4.4
4.2
4
3.8
3.6
3.4
3.2
3
Differential pressure per unit length (kPa/mm)
2
3
4
5
6
7
8
9
10
From port 1 to port n

*Fig. 10*

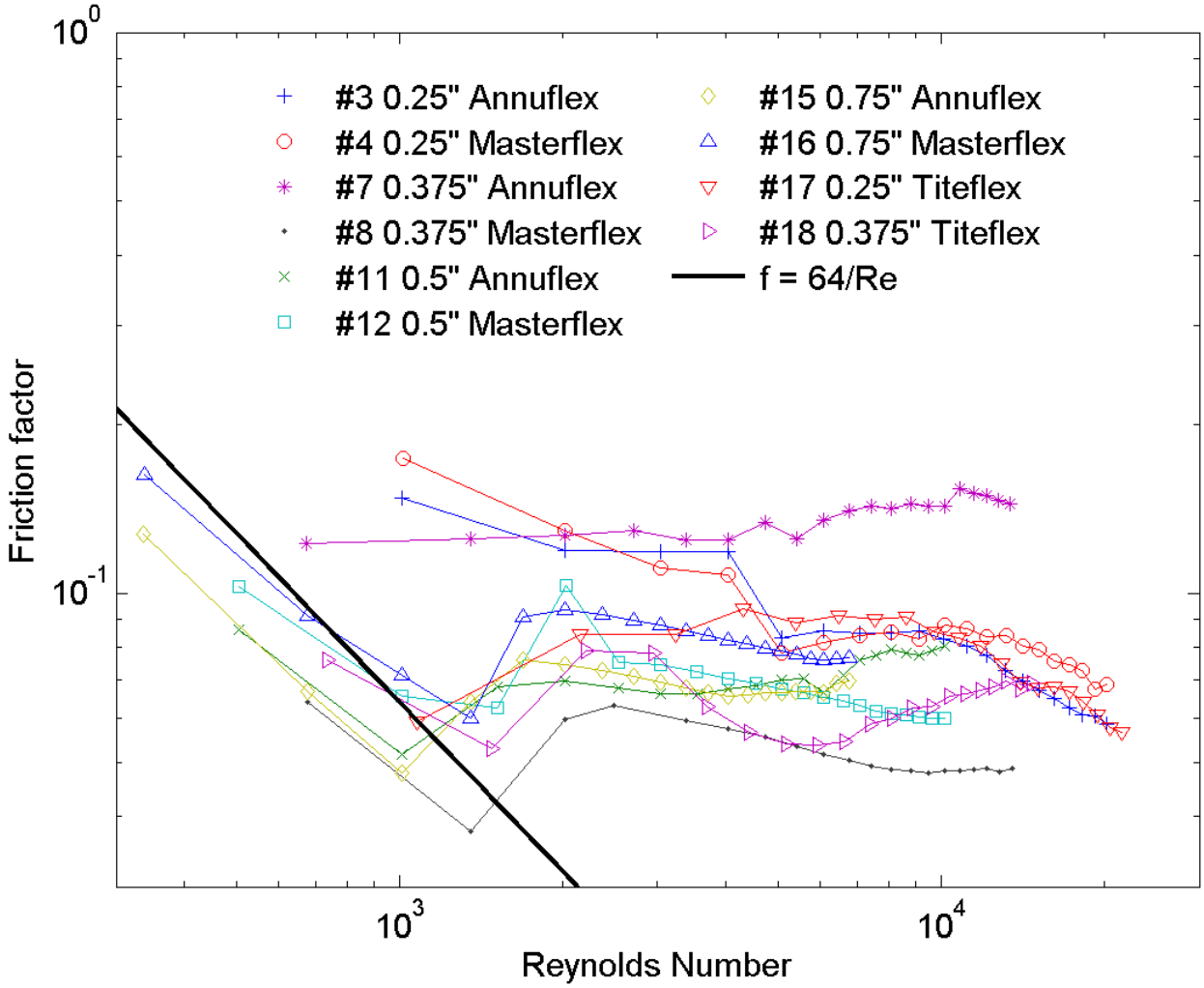
#3 0.25" Annuflex
#4 0.25" Masterflex
#7 0.375" Annuflex
#8 0.375" Masterflex
#11 0.5" Annuflex
#12 0.5" Masterflex
#15 0.75" Annuflex
#16 0.75" Masterflex
#17 0.25" Titeflex
#18 0.375" Titeflex
f = 64/Re
Friction factor
Reynolds Number
10^0
10^-1
10^3
10^4

*Fig. 11*

## Table Caption List

Table 1 Summary of annular corrugated pipes tested

Table 2 Comparison to previous S-type transverse corrugated pipes

Table 3 Pressure Transducer detail

| | Millimeters | | | | | | $Re_{ID}$ | $Re_{OD}$ |
|---|---|---|---|---|---|---|---|---|
| | D (ID) | (OD) | E | P | R | E/D | At 200 scfh | |
| **ANNUFLEX[i]** | | | | | | | | |
| **6.35 (¼")** | 6.35 | 10.41 | 2.03 | 3.07 | 0.77 | 0.320 | 20,295 | 12,375 |
| **9.53 (3/8")** | 9.53 | 15.80 | 3.14 | 3.30 | 0.83 | 0.329 | 13,530 | 8,157 |
| **12.70 (½")** | 12.70 | 19.00 | 3.15 | 4.01 | 1.00 | 0.248 | 10,147 | 6,783 |
| **19.05 (¾")** | 19.05 | 28.93 | 4.94 | 5.72 | 1.43 | 0.259 | 6,765 | 4,455 |
| **MASTERFLEX[j]** | | | | | | | | |
| **6.35 (¼")** | 6.35 | 10.74 | 2.20 | 2.08 | 0.52 | 0.346 | 20,295 | 11,995 |
| **9.53 (3/8")** | 9.53 | 15.77 | 3.12 | 2.06 | 0.51 | 0.327 | 13,530 | 8,170 |
| **12.70 (½")** | 12.70 | 19.18 | 3.24 | 2.44 | 0.61 | 0.255 | 10,147 | 6,720 |
| **19.05 (¾")** | 19.05 | 29.18 | 5.07 | 4.47 | 1.12 | 0.266 | 6,765 | 4,416 |
| **TITEFLEX[k]** | | | | | | | | |
| **6.35 (¼")** | 5.97 | 9.53 | 1.78 | 2.29 | 0.57 | 0.298 | 21,590 | 13,530 |
| **9.53 (3/8")** | 8.71 | 13.54 | 2.41 | 2.41 | 0.60 | 0.277 | 14,792 | 9,519 |

*Table 1*

[i] Provided by Manufacturer
[j] Provided by Manufacturer
[k] These measurements were NOT provided by the manufacturer. They are approximated and measured.

| | $Re_{ID}$[l] | Friction factor | E/D[m] | P/D[n] |
|---|---|---|---|---|
| **Bernhard and Hsieh [9]** | | | | |
| **38.1 mm (1.5”)** | 10,000-110,000 | 0.055-0.065 | 0.0789 | 0.166 |
| **63.5 mm (2.5”)** | | | 0.0484 | 0.123 |
| **Popiel et al. [6]** | | | | |
| **9.53 mm (3/8”)** | 800-10,300 | 0.049-0.093 | 0.148 | 0.462 |
| **12.7 mm (½”)** | 2,700-10,800 | 0.060-0.083 | 0.123 | 0.394 |
| **19.7 mm (1”)** | 4,700-12,000 | 0.055-0.092 | 0.119 | 0.328 |
| **26.7 mm (1.25”)** | 10,000-12,700 | 0.058-0.070 | 0.103 | 0.270 |
| **This study** | | | | |
| **Annuflex 6.35 mm (¼”)** | 1,000-23,000 | 0.058-0.121 | 0.320 | 0.483 |
| **Annuflex 9.53 mm (3/8”)** | 675-13,500 | 0.046-0.105 | 0.329 | 0.346 |
| **Annuflex 12.70 mm (½”)** | 500-10,000 | 0.123-0.144 | 0.248 | 0.316 |
| **Annuflex 19.05 mm (¾”)** | 350-6,750 | 0.04-0.068 | 0.259 | 0.300 |
| **Masterflex 6.35 mm (¼”)** | 1,000-23,000 | 0.058-0.103 | 0.346 | 0.328 |
| **Masterflex 9.53 mm (3/8”)** | 675-13,500 | 0.061-0.102 | 0.327 | 0.216 |
| **Masterflex 12.70 mm (½”)** | 500-10,000 | 0.055-0.201 | 0.255 | 0.192 |
| **Masterflex 19.05 mm (¾”)** | 350-6,750 | 0.072-0.238 | 0.266 | 0.235 |
| **Titeflex 6.35 mm (¼”)** | 400-8,000 | 0.066-0.109 | 0.298 | 0.384 |
| **Titeflex 9.53 mm (3/8”)** | 300-6,150 | 0.056-0.09 | 0.277 | 0.277 |

*Table 2*

[l] Reynolds Number calculated with inner diameter
[m] Relative corrugation depth (E) to inner diameter (D)
[n] Relative corrugation pitch (S) to inner diameter (D)

| Model | Scale Factor (in. $H_2O$/V) | Linearity (% of full scale) | Range (in. $H_2O$) | $((b_{PT})/PT)_{MAX}$ |
|---|---|---|---|---|
| PX654-0.05BD5V | 0.025 | 0.3% | +/- 0.05 | 0.01 |
| PX654-0.5D5V | 0.125 | 0.3% | 0-0.5 | 0.005 |
| PX654-5D5V | 1.125 | 0.3% | 0-5 | 0.005 |
| PX653-50D5V | 12.5 | 0.3% | 0-50 | 0.005 |
| PX656-200DI | 50 | 0.3% | 0-200 | 0.005 |

*Table 3*